



OPEN

Ebselen derivatives inhibit SARS-CoV-2 replication by inhibition of its essential proteases: PL^{pro} and M^{pro} proteases, and nsp14 guanine N7-methyltransferase

Mikolaj Zmudzinski^{1✉}, Wioletta Rut¹, Kamila Olech², Jarosław Granda², Mirosław Giurg², Małgorzata Burda-Grabowska², Rafał Kaleta², Michala Zgarbova³, Renata Kasprzyk^{4,5}, Linlin Zhang⁶, Xinyuanyuan Sun⁶, Zongyang Lv⁷, Digant Nayak⁷, Małgorzata Kesik-Brodacka⁸, Shaun K. Olsen⁷, Jan Weber³, Rolf Hilgenfeld^{6,9}, Jacek Jemielity⁴ & Marcin Drag^{1✉}

Proteases encoded by SARS-CoV-2 constitute a promising target for new therapies against COVID-19. SARS-CoV-2 main protease (M^{pro}, 3CL^{pro}) and papain-like protease (PL^{pro}) are responsible for viral polyprotein cleavage—a process crucial for viral survival and replication. Recently it was shown that 2-phenylbenzisoselenazol-3(2*H*)-one (ebselen), an organoselenium anti-inflammatory small-molecule drug, is a potent, covalent inhibitor of both the proteases and its potency was evaluated in enzymatic and antiviral assays. In this study, we screened a collection of 34 ebselen and ebselen diselenide derivatives for SARS-CoV-2 PL^{pro} and M^{pro} inhibitors. Our studies revealed that ebselen derivatives are potent inhibitors of both the proteases. We identified three PL^{pro} and four M^{pro} inhibitors superior to ebselen. Independently, ebselen was shown to inhibit the N7-methyltransferase activity of SARS-CoV-2 nsp14 protein involved in viral RNA cap modification. Hence, selected compounds were also evaluated as nsp14 inhibitors. In the second part of our work, we employed 11 ebselen analogues—bis(2-carbamoylaryl)phenyl diselenides—in biological assays to evaluate their anti-SARS-CoV-2 activity in Vero E6 cells. We present their antiviral and cytoprotective activity and also low cytotoxicity. Our work shows that ebselen, its derivatives, and diselenide analogues constitute a promising platform for development of new antivirals targeting the SARS-CoV-2 virus.

Abbreviations

Abu	α-Aminobutyric acid
ACC	7-Amino-4-carbamoylmethylcoumarin
DCM	Dichloromethane

¹Department of Chemical Biology and Bioimaging, Wrocław University of Science and Technology, Wyb. Wyspińskiego 27, 50-370 Wrocław, Poland. ²Department of Organic and Medicinal Chemistry, Faculty of Chemistry, Wrocław University of Science and Technology, Wyb. Wyspińskiego 27, 50-370 Wrocław, Poland. ³Institute of Organic Chemistry and Biochemistry, Czech Academy of Sciences, Flemingovo Nám. 2, 16610 Prague, Czech Republic. ⁴Centre of New Technologies, University of Warsaw, Banacha 2C, 02-097 Warsaw, Poland. ⁵College of Inter-Faculty Individual Studies in Mathematics and Natural Sciences, University of Warsaw, Banacha 2C, 02-097 Warsaw, Poland. ⁶Institute of Molecular Medicine, University of Lübeck, Ratzeburger Allee 160, 23562 Lübeck, Germany. ⁷Department of Biochemistry and Structural Biology, University of Texas Health Science Center at San Antonio, San Antonio, TX 78229, USA. ⁸National Medicines Institute, Ul. Chełmska 30/34, 00-725 Warsaw, Poland. ⁹German Center for Infection Research (DZIF), Hamburg-Lübeck-Borstel-Riems Site, University of Lübeck, 23562 Lübeck, Germany. ✉email: mikolaj.zmudzinski@pwr.edu.pl; marcin.drag@pwr.edu.pl

DMF	Dimethylformamide
Et ₃ N	Triethylamine
HMPTA	Hexamethylphosphoramide
MeCN	Acetonitrile
Py-FLINT	Pyrene-based fluorescence intensity
SAM	S-Adenosyl-L-methionine
THF	Tetrahydrofuran
Tle	<i>tert</i> -Leucine

In the winter of 2019, an outbreak of pneumonia with flu-like symptoms emerged in Wuhan, China^{1,2}. Shortly thereafter, the disease-causing pathogen was isolated and analyzed, leading to identification of the novel, highly contagious human beta-coronavirus SARS-CoV-2 (formerly known as 2019-nCoV)³. By February 2023, with over 674 million people diagnosed with Coronavirus Disease 2019 (COVID-19), the death toll exceeded 6.86 million patients worldwide⁴. Newly developed COVID-19 vaccines rely on the immunogenicity of viral spike protein (S), however emergence of novel SARS-CoV-2 Variants of Concerns (VOCs) highlight the need of new antivirals targeting the more conserved non-structural proteins (nsps) of the virus^{5,6}. Various strategies have been employed to accelerate finding an effective therapy to fight the pathogen⁷. One of these strategies is drug repurposing—establishing therapeutic properties for already approved substances for new medical applications. This strategy can be supported by computational analysis, which can lower the costs, speed up the process in comparison with de novo development of new therapeutics and serve as a first stage in screening vast libraries of active compounds^{8–12}. Drug repositioning has already been used in fighting COVID-19¹³. An example here is remdesivir, an antiviral agent targeting the viral RNA-dependent RNA polymerase (RdRp) that was designated to treat Ebola but has shown efficacy in shortening recovery time and reducing mortality as well as serious adverse effects in COVID-19 patients in initial studies¹⁴. However, after extended clinical trials, the WHO Solidarity Trial Consortium concluded that treatment with remdesivir does not prevent, or prevents only a small fraction of, deaths in hospitalized COVID-19 patients. In the study, researchers evaluated also the efficacy of other repurposed drugs—hydroxychloroquine, lopinavir, and interferon beta-1a. As a result, the drugs provided no or little benefit for hospitalized patients with no reduction in hospitalization time, mortality, and initiation of ventilation¹⁵. Recently, two orally administered drugs have been introduced into the market. Pfizer's PF-07321332 (nirmatrelvir) is a SARS-CoV-2 M^{Pro} inhibitor and it is being marketed in combination with Ritonavir under the name paxlovid (<https://clinicaltrials.gov/ct2/show/NCT04960202>; [accessed on 21st Sep 2021]). The second drug, molnupiravir developed by Merck and Ridgeback Biotherapeutics, is a viral RNA-dependent RNA polymerase (RdRp) inhibitor (<https://www.clinicaltrials.gov/ct2/show/NCT04939428>; [accessed on 21st Sep 2021]). Despite this, current treatment options are critically limited and finding new therapeutics for COVID-19 patients constitutes a leading challenge for the scientific community.

To address the problem, scientists identified druggable targets among viral non-structural proteins, two of them being proteases. The SARS-CoV-2 main protease (M^{Pro}, 3CL^{Pro}, nsp5) and the papain-like protease (PL^{Pro}, nsp3 papain-like protease domain) enable viral replication in host cells by processing the viral polyprotein and generating 16 nsps, crucial for virus replication. SARS-CoV-2 M^{Pro} generates 13 viral nsps, making it a key player in the process of virus replication and maturation^{16–18}. M^{Pro} is a cysteine protease with a structure highly conserved among human coronaviruses. In solution, the enzyme exists as both monomers and homodimers, but only the homodimeric form of the protease possesses the full catalytic activity^{18–21}. An unusual preference for a glutamine residue at the P1 position of the substrate cleavage site sets M^{Pro} apart from known human proteases. This feature can be beneficial for design and synthesis of effective, broad-spectrum antiviral agents with minimum side effects^{9,18,19,21–23}. SARS-CoV-2 PL^{Pro} is a viral cysteine protease proposed as an excellent target for COVID-19 treatment due to its pathophysiological roles. PL^{Pro} processes viral polyproteins to generate nsp1–3 proteins. Moreover, the protease also alters the host immune response by deubiquitinating and deISGylating proteins within infected cells^{24–27}. Thus, PL^{Pro} inhibition would not only block the replication of the virus, but would also limit the dysregulation of cellular signaling mediated by ISG15 and ubiquitin.

2-Phenylbenzisoselenazol-3(2*H*)-one (ebselen), firstly prepared by Lesser and Weiß in 1924²⁸, is a small-molecule drug with a pleiotropic mode of action in cells²⁹. Ebselen is an excellent scavenger of ROS that acts as a mimic of the selenoenzyme glutathione peroxidase (GPx) and interacts with the thioredoxin (Trx) system by oxidation of reduced TrxR^{30–32}. During the GPx-like activity, ebselen undergoes a series of reactions arranged in catalytic cycles. Data suggest that the mode of reactions is dependent on the cellular concentrations of thiols and hydrogen peroxide^{30,33–37}. Recently, it was shown that ebselen inhibits both the SARS-CoV-2 proteases. Weglarz-Tomczak et al. evaluated ebselen and a collection of its derivatives as inhibitors of the PL^{Pro}, leading to identification of inhibitors with IC₅₀ values in the nanomolar range³⁸. Ebselen and its derivatives have also been employed in a study by Ampornnanai et al., who investigated the inhibitory effectiveness of these compounds against SARS-CoV-2 M^{Pro} and proposed a mechanism of the enzyme's catalytic Cys145 selenation³⁹. Tested compounds exhibited sub-micromolar IC₅₀ values in recombinant enzyme assays and anti-SARS-CoV-2 activity with EC₅₀ in the low-micromolar range in cellular assays. Moreover, in antiviral assays, ebselen derivatives were superior to ebselen. In another study, a library of approximately 10,000 drugs and drug candidates was screened for M^{Pro} inhibitors. As a result, ebselen displayed the lowest IC₅₀ among the substances tested (0.67 μM), furthermore it also displayed an antiviral effect in SARS-CoV-2-infected Vero cells⁹. In a study by Cao et al. researchers performed HTS of the NIH Clinical Collection compound library. Ebselen was amongst the most potent anticoronaviral agents in cell assays⁴⁰. In a study conducted by Mangiavacchi et al., it was shown that introduction of a selenium atom into the structure of a quercetin derivative increases its antiviral potency

nearly 24 times in comparison with quercetin, indicating the significance of organoselenium compounds in the discovery of novel antivirals⁴¹.

Recent studies revealed that ebselen also inhibits the RNA cap guanine N7-methyltransferase⁴² and exonuclease⁴³ nsp14 activities from SARS-CoV-2. Nsp14 is a bifunctional enzyme with an independently functioning N7-methyltransferase (N7-MTase) domain and an nsp10-dependent exonuclease domain⁴⁴. The enzyme is involved in 5'-end capping of newly synthesized viral mRNAs, crucial for viral transcript stability and protein biosynthesis. The role of nsp14 N7-MTase is to catalyze the reaction of methyl group transfer from *S*-adenosyl-L-methionine (SAM) onto the N7-position of guanosine 5'-triphosphate located at the 5' RNA end (Gppp-RNA), resulting in cap-0 formation⁴⁵. Inhibition of viral N7-MTases has already been shown to suppress viral replication⁴⁵, including that of SARS-CoV⁴⁴. Thus, the nsp14 enzyme is considered a good target for antiviral drug development (Fig. 1)⁴⁶.

The efficacy of ebselen and other organoselenium compounds has been previously evaluated for HIV^{49,50}, HSV2⁵¹, HCV⁵², and Zika virus⁵³ infections. Moreover, a recent report presents ebselen and its derivatives as potent inhibitors of SARS-CoV-2 PL^{pro}³⁸. Currently, ebselen is being evaluated in a phase 2 clinical trials as an oral therapeutic in moderate and severe COVID-19 patients (<https://clinicaltrials.gov/ct2/show/NCT04484025>; <https://clinicaltrials.gov/ct2/show/NCT04483973>; [accessed on 10th Aug 2021]). In this work we investigated ebselen derivatives and analogues as potential anti-SARS-CoV-2 agents. Ebselen's low toxicity and ongoing clinical trials make it attractive as a lead compound. First, we screened a collection of 23 ebselen and 11 ebselen diselenide derivatives and determined the half-maximum inhibitory concentration (IC₅₀) values for the most promising 2-phenylbenziselenazol-3(2*H*)-ones to evaluate their properties as SARS-CoV-2 PL^{pro} and M^{pro} inhibitors. Next, employing a Py-FLINT fluorescence assay, we evaluated nsp14 N7-MTase inhibitory properties for selected ebselen derivatives against the recombinant enzyme. Ebselen's 'open form'—bis[2-(*N*-phenylcarbamoyl)phenyl] diselenide—is proposed as one of the intermediates during ebselen catalytic cycles in living organisms (see Fig. 2) and in cellular environment the compound could act as reservoir of corresponding benziselenazolones

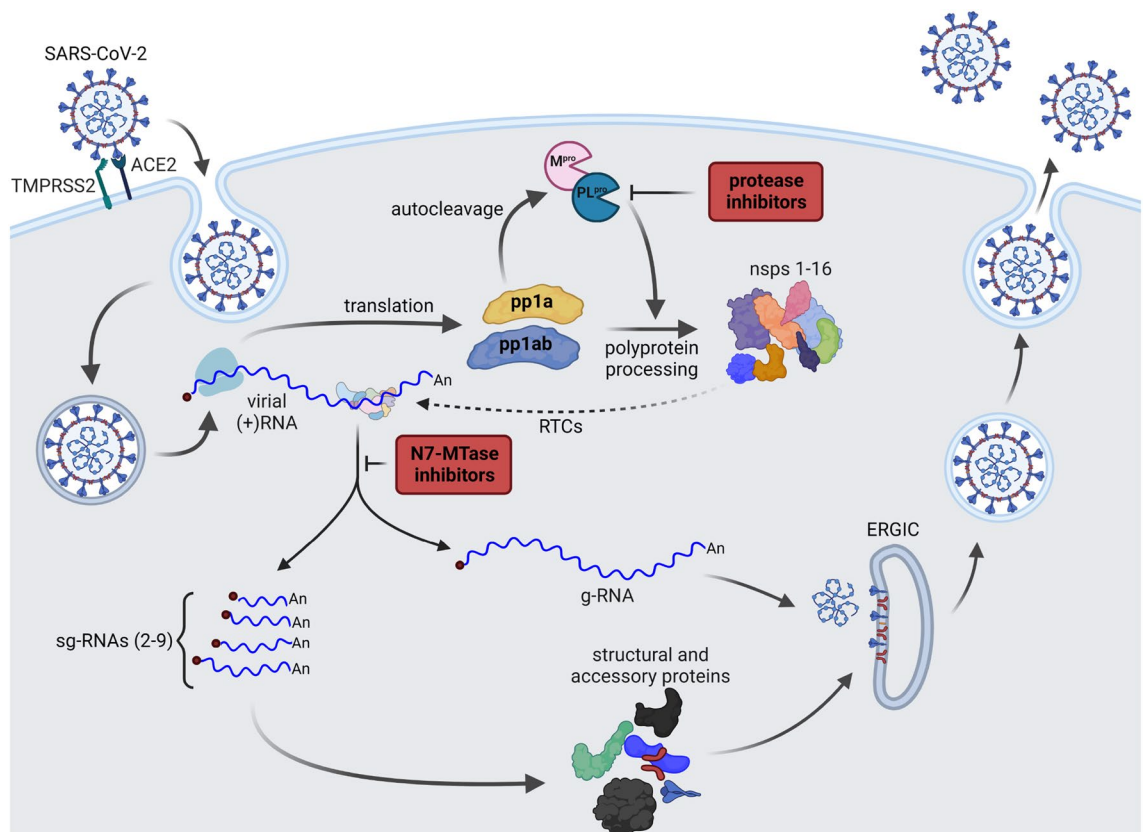


Figure 1. Simplified life cycle of SARS-CoV-2. The virus enters a host's cell and releases its genome in cytoplasm. Viral RNA is translated into two polyproteins: pp1a and pp1ab. Then, due to autocleavage, two viral proteases (PL^{pro} and M^{pro}) are liberated. Their main role is to further process polyproteins, what results in a release of other nsps. Next, a group of nsps form replication and transcription complexes (RTCs). RTCs are further involved in a generation of copies of viral genomic RNA (g-RNA), as well as a set of sub-genomic RNAs (sg-RNA) responsible for synthesis of viral structural and accessory proteins. Virions are assembled in endoplasmic reticulum-Golgi intermediate compartments (ERGICs). g-RNA is coated with structural N-protein and enters the ERGIC containing M, E, and S glycoproteins. Then, the virions are released by exocytosis^{47,48}. Inhibition of M^{pro}, PL^{pro}, and N7-MTase may lead to suppression of virus replication. Protease inhibition stops the generation of nsps, while N7-MTase inhibition prevents the synthesis of stable transcripts of the viral RNA. Created with BioRender.com.

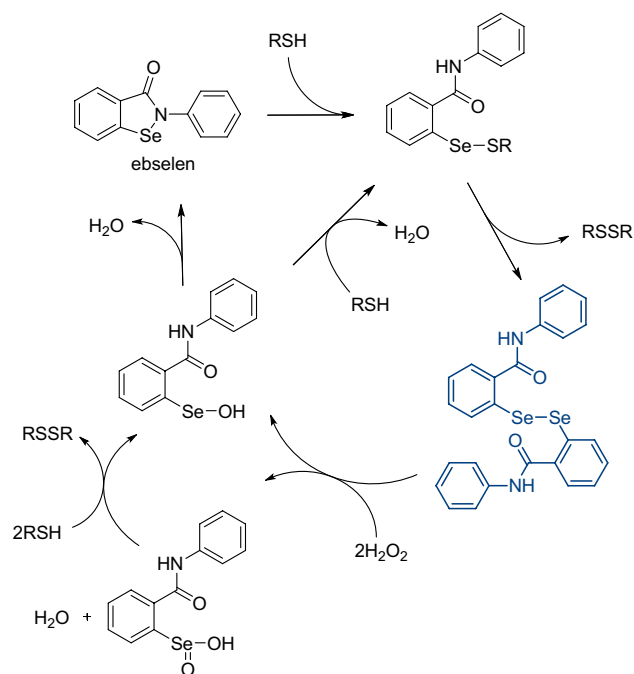


Figure 2. Plausible catalytic cycle of ebselen involving hydrogen peroxide reduction, including formation of the ebselen open form (dark blue color)^{33,37}.

that inhibit viral enzymes and participate in protection against H_2O_2 and other ROS⁵⁴. Hence, we determined anti-SARS-CoV-2 activity in an RNA-reduction-based assay and cytopathic effect-based assays in Vero E6 cells for 11 bis[2-(*N*-arylcarbamoyl)phenyl]diselenides. Lastly, we show that ebselen may constitute a potential lead compound for development of novel antiviral agents with minimal cytotoxic action *in vivo*. The results can be useful in the design of new active compounds targeting the proteases encoded by SARS-CoV-2, to be applied in COVID-19 treatment.

Results and discussion

Compound library preparation. The synthesis of biologically active organoselenium compounds is in the scope of many research teams around the world^{35,55,56}. Ebselen and other benziselenazol-3(2*H*)-ones have been previously prepared by several ways^{57,58}. Structures of compounds included in the collection are presented in Table 1. The general procedure for preparation of ebselen, its derivatives (1–23), and their analogues (24–34) is presented in Fig. 3. 2,2'-dicarboxydiphenyl diselenide (36) was obtained as a result of consecutive protonation, diazotation and disodium or dilithium diselenide selenenylation of anthranilic acid (35). In the next steps, the reactions of diselenide 36 with thionyl chloride in benzene in the presence of DMF at solvent reflux produced 2-(chloroseleno)benzoyl chloride (37) or bis[(2-chlorocarbonyl)phenyl] diselenide (38) depending on the amounts of thionyl chloride used. Tandem selenenylation/acylation reaction⁵⁹ of aniline or its phenyl ring substituted derivatives with 2-(chloroseleno)benzoyl chloride (37) in anhydrous MeCN, or DCM, in the presence of dry Et_3N base gave ebselen and its derivatives 1–23. The acylation reaction of phenyl ring substituted anilines with chloride 38 in anhydrous DCM in the presence of anhydrous Na_2CO_3 as a base gave ebselen 'dimeric' form analogues 25–34⁶⁰. In particular, carbamoylphenyl diselenide 24 was prepared by reduction of ebselen with hydrazine monohydrate in methanol as a solvent⁶¹. The purity of the compounds was >95% as confirmed by LC-MS analysis (see Supplementary Information).

FT-IR spectra were measured in the crystal lattice or in KBr and the 1H -, ^{13}C -, ^{77}Se -, and ^{19}F -NMR spectra were generally measured in $DMSO-d_6$. For ebselen and its analogues 1–23, the wavenumbers corresponding to the stretching vibration of carbonyl (C=O) groups were around 1583–1649 cm^{-1} , nitrogen carbon single bonds with substituent (C-N) bands were at 1305–1363 cm^{-1} , and the C–Se at 727–747 cm^{-1} , moreover, vibration of the diselenides 24–34 are in agreement with data reported previously⁶⁰. In the benziselenazol-3(2*H*)-one region of the NMR spectra measured in $DMSO-d_6$, the proton H-4, H-5, H-6, and H-7 resonances of compound 1–23 were observed at: 7.85–7.94, 7.45–7.51, 7.52–7.78, and 8.05–8.12 ppm, respectively, and the carbon C=O, C-3', C-4, C-5, C-6, C-7 and C–Se resonance generally were observed at 164.87–166.08, 126.43–128.53, 127.73–128.22, 126.06–126.52, 132.07–133.01, 125.71–126.07 and 138.50–140.59 ppm, respectively, while the carbon atom of a phenyl substituent linked with heteroaromatic (PhC-1) resonance was observed at 119.7–146.3 ppm, dependent on the substituents used. The ^{77}Se -NMR resonance of benziselenazolones (1–33) observed at 914.33–974.90 ppm) and diselenides (25–34) observed at 443.48–447.93 ppm) are in agreement with previously published data^{64–66}. For benziselenazolones 1, 14, 15, 17, and 5, we found selenium fluoride spin–spin

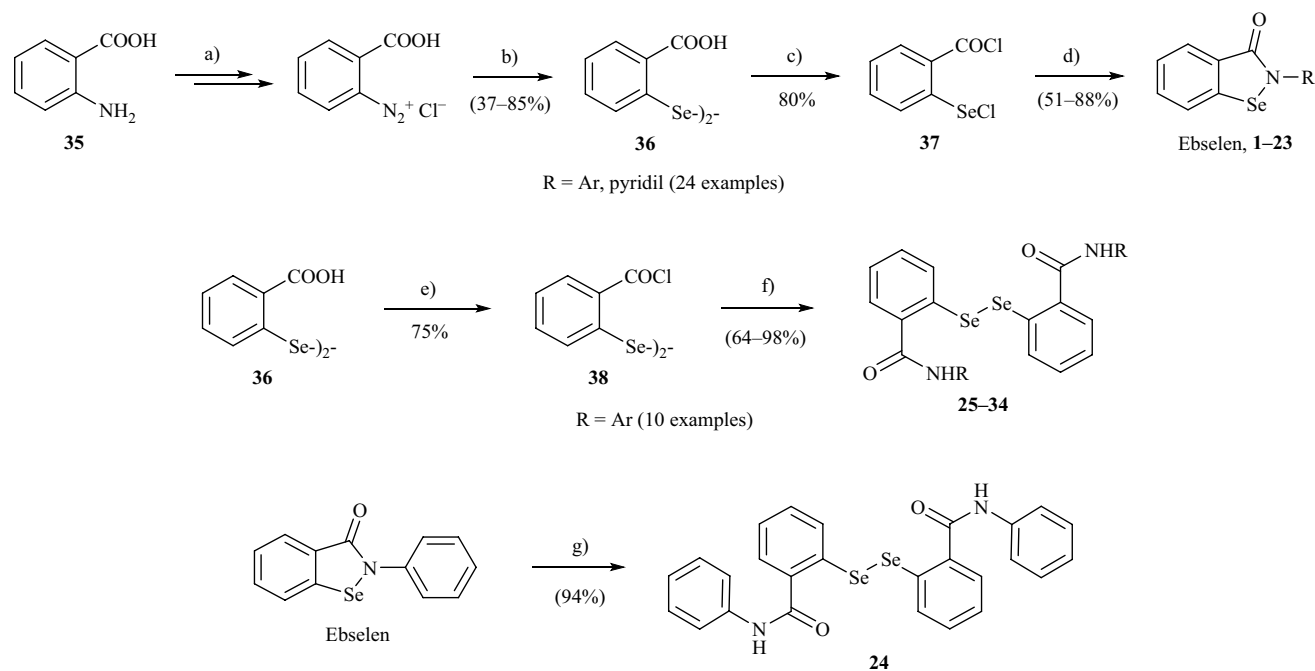


Figure 3. Preparation of ebselen, its derivatives and their ‘dimeric’ form analogues 1–33. Reagents and conditions: (a) (i) aq. HCl, (ii) NaNO₂, –7 to +7 °C, (b) (i) NaSeSeNa, MeOH, NaOH or LiSeSeLi, THF, HMPTA, –7 to +5 °C, (ii) aq. HCl, (c) 7 equiv SOCl₂, cat. (DMF), benzene, reflux, (d) RNH₂, Et₃N, MeCN or DCM, (e) 3.5 equiv SOCl₂, cat. (DMF), benzene, reflux, (f) RNH₂, Na₂CO₃, DCM, (g) H₂N-NH₂·H₂O, MeOH, reflux. (Carried out in accordance with Refs. ^{60,62–64}).

		SARS-CoV-2 PL ^{pro}	SARS-CoV-2 M ^{pro}
		IC ₅₀ (μM)	IC ₅₀ (nM)
Ebselen		1.12 ± 0.06	30.91 ± 2.67
3		1.255 ± 0.10	25.69 ± 2.64
7		0.578 ± 0.04	49.55 ± 2.95
10		1.885 ± 0.10	27.95 ± 5.10
16		0.990 ± 0.06	52.50 ± 4.51
17		2.067 ± 0.08	15.24 ± 4.58
20		1.038 ± 0.08	37.81 ± 3.28
21		1.288 ± 0.05	27.37 ± 2.35

Table 2. Inhibitory activity of ebselen and its selected derivatives against SARS-CoV-2 PL^{pro} and M^{pro}. For IC₅₀ graphs see Supplementary Information Fig. S1. Significant values are in bold.

only investigated ebselen derivative with a 3-substituted pyridinyl moiety instead of a substituted phenyl ring. For the M^{pro}, the best hits were compounds **10** and **17**. Compound **10** represents monosubstituted derivatives with a nitro group at the *para* position, while **17** is a derivative with 2-fluoro and 5-chloro substitutions in the aromatic ring. We observed that 2,4-dimethoxy derivative **16** displays potency towards both of the proteases close to that of ebselen, however, in comparison with ebselen, its toxicity evaluated in the A549 human cell line was 10 times lower⁶⁰. In general, substitutions within the phenyl ring of ebselen boost inhibition of M^{pro} as we identified only 3 compounds (**6**, **7** and **12**) with a potency lower than for ebselen. See Table S2 in supplementary information for screening results³⁹.

Based on the screening results, we selected ebselen and seven of its derivatives for further inhibitory property evaluation in IC₅₀ assays. We chose compounds: (a), exhibiting the highest potency towards M^{pro} (**10**, **17**) or PL^{pro} (**7**) in the screening; or (b), displaying relatively high inhibition towards both the investigated proteases (**3**, **16**, **20**, **21**). During the assays, IC₅₀ values for PL^{pro} were in the micromolar range while for M^{pro}, they were in the low nanomolar range. The results are presented in Table 2. For the reference inhibitor, ebselen, IC₅₀ values were 1.12 ± 0.06 μM for PL^{pro} and 30.91 ± 2.67 nM for M^{pro}. Compound **7**, which was the best hit in the PL^{pro} inhibitor screening assay, indeed had the lowest IC₅₀ value (0.58 ± 0.04 μM) among the tested compounds. Despite ebselen being the second best PL^{pro} inhibitor in the screening assay, we found that two other compounds (**17**, **21**) displayed slightly lower IC₅₀ values. Compounds **10** and **17**, which were selected for the analysis as the best M^{pro} inhibitors, displayed lower IC₅₀ values than ebselen. The most potent M^{pro} inhibitor with IC₅₀ = 15.24 nM was compound **17**, the second best hit from the screening experiment. Interestingly, the best hit **10** displayed an IC₅₀ value similar to values determined for **3** and **21** (27.95 nM, 25.69 nM, and 27.37 nM respectively). For **16** and **20**, we observed that despite a higher potency in the screening assay, the IC₅₀ values determined for these compounds were higher than for ebselen.

IC₅₀ is an assay-dependent measure. Low IC₅₀ values obtained for the compounds are probably due to the used substrates' properties. SARS-CoV-2 PL^{pro} possesses deubiquitinating activity and used Ac-LRGG-ACC substrate has relatively low k_{cat}/K_M value ($k_{cat}/K_M \approx 900 \text{ s}^{-1} \text{ M}^{-1}$). Optimal substrates for this enzyme are based on ubiquitin or ISG15 molecules²⁶. For SARS-CoV-2 M^{pro} we used our novel tetrapeptide QS1 fluorogenic substrate, that has a lower k_{cat}/K_M value ($k_{cat}/K_M = 859 \text{ s}^{-1} \text{ M}^{-1}$) in comparison to FRET substrates²².

Inhibition of nsp14 N7-MTase by 2-phenylbenziselenazol-3(2H)-ones. Selected ebselen analogues—**3**, **7**, **10**, **16**, and **17** were further tested for their inhibitory properties towards nsp14 N7-MTase. To determine their IC₅₀ values, we used the previously described fluorescence assay Py-FLINT^{42,67}. To this end, the Py-FLINT probe (1 μM) was incubated with SAM cosubstrate (20 μM), nsp14 enzyme (40 nM), and half-log inhibitor dilutions in 50 mM Tris-HCl pH 7.5 buffer at 30 °C. The reaction progress was monitored in 96-well cells by registering the fluorescence intensity signal with a 1-min time interval. Using the initial reaction course, the values of initial rates *V* were calculated. To calculate IC₅₀ values from the obtained dependences of initial rates versus inhibitor concentration, we fitted a four-parameter dose-response equation, assuming a variable Hill slope *p* (Table 3, Fig. S2).

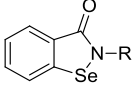
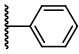
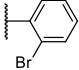
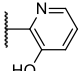
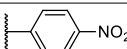
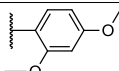
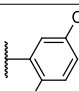
		SARS-CoV-2 nsp14	
		IC ₅₀ (μM)	<i>p</i>
Ebselen		0.35 ± 0.03	2.74 ± 0.47
3		0.35 ± 0.02	3.12 ± 0.47
7		0.35 ± 0.02	4.08 ± 1.33
10		3.08 ± 0.46	1.73 ± 0.35
16		0.42 ± 0.04	2.36 ± 0.32
17		3.83 ± 0.35	2.15 ± 0.28

Table 3. IC₅₀ and Hill coefficient (*p*) values determined for SARS-CoV-2 nsp14 N7-MTase using the Py-FLINT assay. For inhibition curves see Supplementary Information Fig. S2. Significant values are in bold.

High values of the hill slope were observed for the most potent inhibitors (compounds **3**, **7** and ebselen control) and we assume that they result from limitations of applied fluorescent method. The range of inhibition that can be studied in competition experiment is limited by the fluorescent probe affinity to the protein. We believe that a better fluorescent substrate with lower Michaelis-Menten constant value would enable better distinguishment between strong nsp14 inhibitors visible in $p \sim 1$. Compounds **3**, **7** and **16** had IC_{50} values comparable to ebselen (0.35–0.42 μM), indicating they are potent inhibitors of nsp14. Compounds carrying 4-nitrophenyl (**10**) and 5-chloro-2-fluorophenyl (**17**) substitutions had one order of magnitude higher IC_{50} values ($3.08 \pm 0.46 \mu\text{M}$ and $3.83 \pm 0.35 \mu\text{M}$, respectively). The same substitutions caused an increase in inhibitory potency against M^{pro} , which implies that phenyl ring substitutions are a possible route towards tailoring selectivity of the compounds. Overall, the results indicate that ebselen and its derivatives may act as multi-target inhibitors of SARS-CoV-2 protein activity.

Ebselen diselenide derivatives as SARS-CoV-2 M^{pro} , PL^{pro} , and nsp14 inhibitors. To get a deeper insight into the biological activity of organoselenium compounds, we included a collection of 11 diselenides—open forms of various ebselen derivatives in our study. First, we performed a screening for PL^{pro} and M^{pro} inhibitors according to a protocol employed for benzenoselenazol-3(2*H*)-ones. Screening revealed that diselenides inhibit both of the proteases. Diselenides generally inhibited M^{pro} more poorly than ebselen; however, contrary to benzenoselenazolones, for PL^{pro} , diselenides displayed a higher potency than the reference compound (for full screening results see Supplementary Information Table S3). The IC_{50} parameter for protease inhibition could not be assessed due to the high hydrophobicity of the compounds and their precipitation in the assay buffer. Next, we tested diselenides for anti-N7-MTase activity employing the Py-FLINT assay. All of the tested compounds displayed IC_{50} values in the high nanomolar or low micromolar range (Table 4). We observed that for compound **25** with a 2-fluorosubstituted phenyl ring, the IC_{50} is 3 times lower ($0.12 \pm 0.01 \mu\text{M}$) than for ebselen. The ‘dimeric form’ of ebselen **24** and its 3-fluorosubstituted derivative **27** also displayed an IC_{50} around two times lower than ebselen. Results for these compounds correlate with their low EC_{50} values in CPE and RNA-based assays (Table 5).

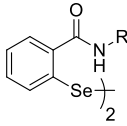
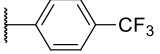
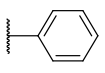
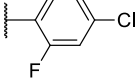
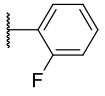
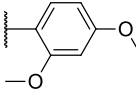
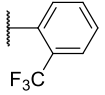
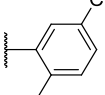
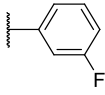
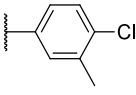
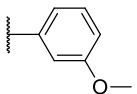
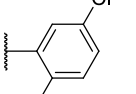
					
IC_{50} (μM)		IC_{50} (μM)			
R:		SARS-CoV-2 nsp14	R:	SARS-CoV-2 nsp14	
Ebselen		0.35 ± 0.03	29 	4.5 ± 1.3	
24		0.21 ± 0.02	30 	11.5 ± 1.4	
25		0.12 ± 0.01	31 	0.91 ± 0.10	
26		1.82 ± 0.32	32 	12.1 ± 1.1	
27		0.18 ± 0.04	33 	1.06 ± 0.05	
28		0.58 ± 0.04	34 	2.10 ± 0.58	

Table 4. Ebselen diselenide derivatives as SARS-CoV-2 nsp14 inhibitors. IC_{50} was determined in the Py-FLINT assay. Conditions: probe $[S_1] = 1 \mu\text{M}$, SAM cosubstrate $[S_2] = 20 \mu\text{M}$, nsp14 $[E] = 40 \text{ nM}$. For inhibition curves see Supplementary Information Fig. S3. Significant values are in bold.

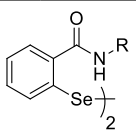
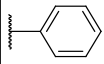
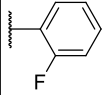
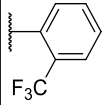
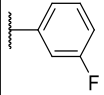
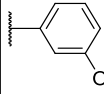
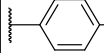
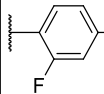
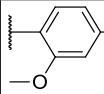
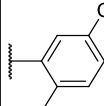
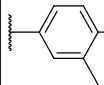
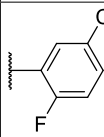
					
R:		EC ₅₀ (μM) CPE	EC ₅₀ (μM) RNA	Titer reduction at EC ₉₀ (log ₁₀ PFU/mL)	CC ₅₀ (μM)
Ebselen		34 ± 7.9	n.d.	n.d.	~ 30
24		1.5 ± 0.13	1.0 ± 0.14	1.5	> 50
25		3.1 ± 0.36	1.9 ± 0.15	3.3	~ 60
26		37 ± 2.4	n.d.	n.d.	> 50
27		0.7 ± 0.13	1.5 ± 0.15	0.4	> 50
28		7.6 ± 0.71	2.7 ± 0.23	0.5	> 50
29		29 ± 3.5	n.d.	n.d.	> 50
30		1.1 ± 0.15	1.9 ± 0.1	1.1	> 50
31		7.1 ± 0.84	2.8 ± 0.31	0.3	> 50
32		22 ± 2.5	n.d.	n.d.	> 50
33		20 ± 1.4	1.7 ± 0.08	0.3	> 50
34		9.3 ± 0.92	3.4 ± 0.2	1.3	> 50
Remdesivir		0.1 ± 0.01	0.66 ± 0.06	3.1	> 50

Table 5. Anti-SARS-CoV-2 activities (EC₅₀) and cytotoxicity in Vero E6 cells (CC₅₀) for investigated diselenides determined by RNA reduction- and CPE-based assays. Remdesivir was used as a positive control. For inhibition curves see Supplementary Information Figs. S4–S6. *n.d.* not determined, *CPE* cytopathic effect-based assay, *RNA* RNA reduction-based assay, *PFU* plaque forming units. Significant values are in bold.

Evaluation of ebselen diselenide derivatives: anti-SARS-CoV-2 activity in Vero E6 cells. In vitro assays with recombinant enzymes showed that ebselen, its derivatives, and analogues possess inhibitory activity towards SARS-CoV-2 M^{pro}, PL^{pro}, and nsp14. Knowing that ebselen diselenide takes part in ebselen's catalytic cycles and that oxidative stress plays an important role in SARS-CoV-2 infection⁶⁸, we assumed that ebselen analogues—bis(2-carbamoylaryl)phenyl diselenides—could also possess antiviral activity in cells. Our next step was the evaluation of antiviral properties and cytotoxicity of selected ebselen analogues in cellulo in the Vero E6 cell line⁶⁹. For this experiment, we included the available dimeric forms of ebselen derivatives (structures presented in Table 5). To get a deeper insight into the activity of tested compounds, we performed four tests:

cytopathic effect-based assay, RNA reduction-based assay, virus titer reduction assay, and cytotoxicity assay. Compounds with an EC_{50} higher than 20 μM in the CPE-based assay were excluded from the RNA reduction-based and virus titer reduction assays. We used remdesivir as a positive control anti-SARS-CoV-2 agent. Besides ebselen, the CC_{50} of all tested compounds exceeded 50 μM , indicating their generally low cytotoxicity. Moreover, ebselen displayed the second highest EC_{50} in the CPE-based assay. However, for ebselen diselenide (bis(2-carbamoyl)diphenyl diselenide, **24**), we observed the strongest antiviral response ($EC_{50} = 1.0 \pm 0.14 \mu\text{M}$ in the RNA reduction-based assay) and the third strongest cytoprotective effect ($EC_{50} = 1.5 \pm 0.13 \mu\text{M}$ in the CPE-based assay). The highest cytoprotective effect was observed for bis[2-(3-fluorophenylcarbamoyl)]phenyl diselenide (**27**), which was the only diselenide with EC_{50} in the nanomolar range ($EC_{50} = 0.7 \pm 0.13 \mu\text{M}$). The compound also displayed high antiviral activity with the second lowest EC_{50} ($1.5 \pm 0.15 \mu\text{M}$) in the RNA reduction-based assay. Another potent compound was **30**, with a 4-chloro and 2-fluoro substituted phenyl ring, as it displayed the second lowest EC_{50} in the CPE-based assay. In most cases, we observed that for diselenides with methyl (**32** and **33**, with chlorine counterparts) or larger substituents (**28**, **31**—methoxy, and **26**, **29**—trifluoromethyl groups), the cytoprotective effect was decreased, but the antiviral activity did not change significantly compared to compounds with only halide substituents in the phenyl ring. However, compound **34** with a 5-chloro-2-fluoro substituted phenyl ring displayed the highest EC_{50} in the RNA reduction-based assay and had considerably higher EC_{50} in the CPE-based assay compared to other halide-substituted ebselen diselenide derivatives (**25**, **27**, **30**). We observed that especially trifluoromethyl groups hampered the activity of the compounds, resulting in the highest EC_{50} values in the CPE-based assay. The anti-SARS-CoV-2 potency of diselenide derivatives was further confirmed by the determination of maximum virus titer reduction at EC_{90} concentration. The virus titer reduction ranged from 0.3 to 3.3 \log_{10} PFU/mL with the compound **25** displaying the best virus titer reduction followed by compound **24**, **34**, and **30**.

Conclusions

With over 6.86 million deaths caused by COVID-19, the need for a widely accessible, effective and safe therapy against coronaviral diseases is crucial for public health. A promising strategy involves M^{pro} inhibition and this approach can lead to novel, broad spectrum anticoronaviral drugs¹⁸. Recently, repurposing efforts enabled identification of ebselen as a potential drug against COVID-19, probably due to its action as an inhibitor of the SARS-CoV-2 main protease⁹. This concept was later supported by Ampornanai et al., who proposed a mechanism for selenation of M^{pro} 's catalytic Cys145 residue by ebselen³⁹. Furthermore, using molecular dynamics simulations, Menéndez et al. explored noncovalent interactions between the M^{pro} and the ebselen molecule. Researchers found two possible interaction sites: one located within the active site and the second in the region involved in dimer formation⁷⁰. Promising results coming from studies of ebselen as anti-SARS-CoV-2 agent inspired researchers to explore also its derivatives as potential antivirals. Węglarz-Tomczak et al. investigated ebselen and its analogues as PL^{pro} protease inhibitors³⁸. Qiao et al. designed and synthesized a series of ebselen derivatives to improve the inhibition of the SARS-CoV-2 M^{pro} . Researchers identified three compounds, that were superior to ebselen in cellular antiviral activity assays performed in HPAepiC cells⁷¹. Sun et al. investigated ebselen, ebsulfur and their derivatives as M^{pro} inhibitors. In non-reducing conditions all of the compounds displayed inhibitory properties. However, the inhibition was diminished in DTT-dependent screening assay, what led to the conclusion, that ebselen is a promiscuous cysteine protease inhibitor and its antiviral activity in cells may not be a result of direct protease inhibition. The role of ebselen as a protease inhibitor has been also questioned by Ma et al., who showed, that ebselen binds nonspecifically to active sites of various cysteine proteases in the lack of reducing agent⁷². In another study by the Wang's group ebselen displayed no M^{pro} inhibition in cells in Protease-Glo luciferase and Flip-GFP assays. Authors performed in vitro FRET substrate assay using recombinant enzyme and showed, that in presence of reducing agent ebselen does not inhibit the protease⁷³. Additionally, employing Flip-GFP assay, researchers observed no SARS-CoV-2 PL^{pro} inhibition by ebselen in 293T-ACE2 cells⁷⁴. No cellular M^{pro} inhibition was reported also by Heilmann and colleagues, who developed a novel, VSV-based assay for evaluation of protease inhibitors in cells⁷⁵.

Ebselen has a pleiotropic mode of action that is a result of its reactivity towards cysteine residues affecting many biological targets^{29,31,76}. One of the plausible explanations for high antiviral activity of ebselen and its derivatives might be their function as mimetics of GPx selenoenzymes, that are crucial in maintaining low levels of ROS (Fig. 2). The oxidative stress plays a major role in viral infections⁷⁷, thus, antioxidants such as organoselenium compounds may provide a beneficial outcome. What is more, the GPx1 isoform was proposed as a possible SARS-CoV-2 M^{pro} cellular substrate, thus presence of ebselen in cells would counteract the depletion of the enzyme⁷⁸. Additionally, Du et al. have shown, that SARS-CoV-2 M^{pro} activity might be promoted by the oxidative stress⁷⁹. Thus, antioxidant activity of ebselen would indirectly decrease the activity of SARS-CoV-2 M^{pro} , however, this concept needs further investigation and experimental confirmation.

Organoselenium compounds may display toxicity at higher concentrations due to their pan-reactivity toward thiol groups⁷⁶. However, the clinical safety of ebselen has been proven in multiple studies what makes this substance a good candidate for further structure optimization. Ebselen belongs to the NIH Clinical Collection compound library, that gathers substances that are not currently clinically used, but with history of usage in clinical trials in humans. Its efficacy and safety in humans have been evaluated in various studies. In a phase I clinical trial of ebselen as a potential treatment for hearing loss in humans, patients tolerated a single dose of 1600 mg⁸⁰. In a phase IIa double-blind placebo study of ebselen in treatment of mania or hypomania, the drug was administered for three weeks in 600 mg doses. As an outcome, adverse effects in both groups were comparable⁸¹. Administration of ebselen for two weeks in doses of 300 mg a day also was proven to be safe for patients suffering from acute ischemic stroke⁸². Eventually, due to its favorable pharmacokinetics and safety profile, ebselen is being investigated as a safer alternative to lithium salts in bipolar disorder⁸³.

In our study, we utilized a collection of ebselen derivatives and analogues to evaluate their SARS-CoV-2 PL^{pro} and M^{pro} inhibitory properties. As ebselen has been identified as a potent nsp14 N7-MTase inhibitor, we also evaluated our series of ebselen analogues against SARS-CoV-2 nsp14. First, we screened a library of organoselenium compounds. Next, we determined IC₅₀ values for selected compounds. The most potent PL^{pro} inhibitor, 2-(3-hydroxypyridin-2-yl)-1,2-benzisoselenazol-3(2H)-one, displayed the highest potency in the screening assay and the lowest IC₅₀ value (0.58 μM). IC₅₀ determination enabled identification of two more compounds with inhibitory properties similar to ebselen. These compounds were 2,4- and 2,5- disubstituted derivatives of ebselen that displayed lower potency during screening, but also slightly lower IC₅₀ parameters than for the reference inhibitor. A similar analysis for the M^{pro} enabled identification of four compounds displaying higher potency during screening and a lower IC₅₀ parameter. Two of them had a monosubstituted phenyl ring at the *para* and *ortho* positions, and two were disubstituted ebselen derivatives. The best inhibitor with an IC₅₀ value approximately 2 times lower than for ebselen was 2-(5-chloro-2-fluorophenyl)-1,2-benzisoselenazol-3(2H)-one. Among the ebselen derivatives tested, we found compounds with 2-bromophenyl and 2-(3-hydroxypyridin-2-yl) modifications having inhibitory properties towards nsp14 similar to ebselen.

Another part of the research was assessment of antiviral and cytoprotective activity of ebselen and its diselenide analogues. We tested 12 selenoorganic compounds and remdesivir (positive control) in Vero E6 cells. CPE and RNA reduction-based assays revealed that this class of compounds could be a source of promising candidates for new antiviral agents. Cytotoxicity of the diselenides was generally low (CC₅₀ > 50 μM). We observed that for ebselen diselenide and 3 out of 4 diselenides with halogen substitutions in the phenyl ring, EC₅₀ in the CPE reduction-based assays was the lowest. Ebselen diselenide also displayed the highest antiviral activity in the RNA reduction-based assay. Substitution with bigger groups resulted in lower cytoprotective activity (higher EC₅₀ in the CPE reduction-based assay), but a similar effect was not observed for antiviral activity.

In this work, we showed that in non-reducing conditions ebselen derivatives with substitutions and other modifications within the phenyl ring generally possess good inhibitory properties against both of the proteases and the N7-guanine methyltransferase encoded by the novel coronavirus in *in vitro* assays. Moreover, ebselen diselenide derivatives possess high antiviral and cytoprotective activity. The results constitute a promising platform for novel therapeutics and we believe that the data can be used to facilitate efforts towards new anticoronaviral drugs to be used for the treatment of COVID-19.

Materials and methods

Compound library preparation. All solvents were distilled before use. Commercially available reagents were used without further purification. Selenium powder (100 mesh) (Sigma-Aldrich, Saint Louis, MO, USA) used for Na₂Se₂ and Li₂Se₂ preparation had a purity of ≥ 99.5%. Freshly distilled MeCN was redistilled twice over P₂O₅ before preparation of ebselen and its derivatives. MeOH was distilled slowly over a mixture of LAH and CaH₂ before hydrogenation of ebselen. CH₂Cl₂ (DCM) was distilled over P₂O₅ before preparation of ebselen analogues 25–34. Triethyl amine (Et₃N) (POCh, Gliwice, Poland), distilled over NaOH, was stored over NaOH pellets. Anhydrous sodium carbonate (Na₂CO₃) (POCh, Gliwice, Poland) was ground in a mortar before use. The intermediates, 2-(chloroseleno)benzoyl chloride and bis[(2-chlorocarbonyl)phenyl] diselenide were prepared from anthranilic acid and elemental selenium via the formation of 2,2'-dicarboxyphenyl diselenide—a key intermediate, according to the literature procedure^{60,61,63,64}. Preparative column chromatography was performed on Merck Si60 silica gel (63–200 μm). Analytical TLC was performed on PET foils precoated with silica gel (Merck silica gel, 60 F254) (Sigma-Aldrich, Saint Louis, MO, USA), and were visualized with light (λ_{max} = 254 nm), or by staining with iodine steam. Melting points were determined on an Electrothermal IA 91100 digital melting-point apparatus using the standard open capillary method. IR spectra (4000–400 cm⁻¹) were recorded in KBr plates on a Perkin-Elmer 2000 FT-IR spectrometer or on a Fourier transform, Bruker VERTEX 70V spectrometer using diamond ATR accessory. Absorption maxima are reported in wavenumbers (cm⁻¹). ¹H-NMR and ¹³C-NMR spectra (300.1, 399.8, 600.6 MHz and 75.48, 100.5, 151.0 MHz, respectively) were recorded on a Bruker DRX 300 (Bruker, Rheinstetten, Germany), Jeol 400yh (Jeol, Tokyo, Japan) and Bruker Avance II 600 (Bruker, Poznań, Poland) instruments. NMR spectra recorded in CHCl₃-d₁ and DMSO-d₆ were referenced to the respective residual ¹H or ¹³C signals of the solvents, and chemical shifts (δ) are given in parts per million (ppm), and coupling constants (*J*) are in Hz. ¹⁹F-NMR and ⁷⁷Se-NMR (376.2 and 76.24 MHz, respectively) were collected on Jeol 400yh instrument. High-resolution mass spectra were collected using electrospray ionization on a Waters LCT Premier XE TOF instrument.

The literature procedure was adapted for the preparation of dilithium diselenide⁶², diaryl diselenides 24⁸⁴, 28^{60,63}, 31⁶⁰, 32–33⁶³, 36^{60,64}, 38⁶⁰, and 2-(chloroseleno)benzoyl chloride (37)⁶⁰. Purity and homogeneity of known compounds were confirmed by measuring their m.p. for ebselen⁶⁰, 1–2⁵⁸, 3⁵⁷, 7–8⁶⁰, 9⁸⁵, 11⁸⁶, 16⁶⁰, 19–22⁶³, 23⁶⁰, 24⁸⁷, 26⁸⁷, 28⁶³, 29⁸⁷, 31⁶⁰, 32–33⁶³, 36⁸⁶, 37⁸⁸, and 38⁸⁶, or FT-IR spectra for ebselen⁵⁷, 3⁵⁷, 10⁶⁶, 11⁸⁶, 16⁶⁰, 31⁶⁰, ¹H- and/or ¹³C-NMR spectra for 1–2⁵⁸, 7^{59,60}, 8⁶³, 10⁸⁶, 11⁸⁶, 16⁶⁰, 19–22⁶³, 23⁶⁰, 24⁸⁴, 28⁶³, 31⁶⁰, 32⁶³, and ⁷⁷Se-NMR spectrum for 10⁶⁶, and HRMS for 16⁶⁰, and comparing them with literature data. All new 13, 30, 34, uncharacterized, 4⁸⁹, 5⁸⁷, 6⁹⁰, 9⁸⁵, 12⁹¹, 14⁹¹, 15⁹², 17–18⁹³, 25⁹², 27⁹², and spectroscopically uncharacterized 26, 29⁸⁷ selenium species were fully characterized. The hydrogen and carbon atom positions in the ¹H-NMR and ¹³C-NMR spectra were supported by the dept-135 or COSY experiments and by 2D-NMR map analysis of the Heteronuclear Multiple-Quantum Correlation (HMQC) and Heteronuclear Multiple Bond Correlation (HMBC), Nuclear Overhauser Enhancement Spectroscopy (NOESY) if measured. See Supporting Information for detailed synthesis protocols and compounds spectroscopic characterization.

SARS-CoV-2 PL^{pro} preparation. SARS-CoV-2 PL^{pro} was prepared as described²⁶. In brief, *pGEX6P-1-SARS-CoV-2PLpro* was transformed into BL21 (DE3) codon-plus *E. coli* cells and induced with 0.1 mM IPTG

and 0.1 mM ZnSO₄ at 18 °C overnight. GST-fusion SARS-CoV-2 PL^{Pro} was purified using a standard protocol. The fusion protein was cleaved using GST-PreScission protease at 4 °C overnight followed with desalting and passing through fresh glutathione beads to remove cleaved GST and GST-PreScission protease. The sample was further purified using Superdex 200 pg size-exclusion columns (GE) equilibrated with 20 mM Tris–Cl pH 8.0, 40 mM NaCl and 2 mM DTT. The peak fractions were pooled and concentrated to ~10 mg/mL and snap frozen in liquid nitrogen for later use.

SARS-CoV-2 M^{Pro} preparation. SARS-CoV-2 M^{Pro} was recombinantly produced as described¹⁸. Briefly, the gene of the M^{Pro} was cloned into the PGEX-6p-1 vector, which has a Nsp4-Nsp5 and a PreScission cleavage site at the N- and C-termini, respectively, to generate the authentic target protein. The gene of the target protein was expressed in the *E. coli* of the BL21-Gold (DE3) (Novagen) strain. The recombinantly produced M^{Pro} was purified by employing HisTrap FF (GE Healthcare) and ion-exchange chromatography (Q FF, GE Healthcare). Finally, the high-purity target protein was subjected to a buffer exchange (20 mM Tris, 150 mM NaCl, 1 mM EDTA, 1 mM DTT, pH 7.8) for further experiments.

SARS-CoV-2 nsp14 preparation. SARS-CoV-2 mRNA cap guanine N7-methyltransferase nsp14 was prepared as described previously⁴². Briefly, the nsp14 gene was cloned into the pET28 SUMO expression vector. Nsp14 was overexpressed in BL21 (DE3) RIL *E. coli* (Invitrogen), as a fusion protein with His-tagged SUMO. The fusion protein was purified using HisTrap FFTM column (Cytiva), followed by loading on HiTrap 26/10 Desalting column (Cytiva). To remove the N-terminal tag (6×His-Sumo) Sumo protease (MCLAB) was added and then the nsp14 protein again purified on HisTrap FFTM column. Flow-through fractions containing nsp14 were collected and separated from N-terminal tag (6×His-Sumo), and His-tagged Sumo protease. The flow-through fraction was further finally purified on a Superdex 75 pg HiLoad 26/600 gel filtration column (Cytiva). Fractions containing nsp14 were concentrated to 30 μM, flash frozen and stored at –80 °C in a buffer containing 50 mM HEPES (pH 8.0), 100 mM NaCl, 1 mM DTT, 10% glycerol.

Inhibitor screening. Evaluation of the compound library for inhibitors of SARS-CoV-2 PL^{Pro} and SARS-CoV-2 M^{Pro} was carried out in Corning 96-wells plates. For PL^{Pro}, 1 μL of each compound in DMSO solution was added to the wells. Next, 79 μL of enzyme preincubated for 10 min at 37 °C in assay buffer (50 mM Tris, 5 mM NaCl, 0.075% BSA, pH 7.5) was added to each well. The enzyme was incubated with the compounds at 37 °C for 30 min. Next, 20 μL Ac-LRGG-ACC substrate in assay buffer was added to the wells. Final concentrations were: 100 nM enzyme, 10 μM substrate and 1 μM tested compounds. In the assay for M^{Pro}, 1 μL of each compound in DMSO solution was added to the wells. Next, 79 μL of enzyme in assay buffer (50 mM Tris, 1 mM EDTA, pH 7.3)⁹⁴ was added to each well and the plate was incubated at room temperature for 2 min. Next, 20 μL of QS1 substrate in assay buffer was added to the wells. Final concentrations were: 100 nM enzyme, 50 μM substrate, and 100 nM or 1 μM tested compounds. Measurements were carried out at 37 °C using a Molecular Devices Spectramax Gemini XPS spectrofluorometer. ACC fluorophore release was monitored for 30 min ($\lambda_{\text{ex}} = 355$ nm, $\lambda_{\text{em}} = 460$ nm). For the further analysis, the linear range of the progress curves was used. Measurements were performed at least in duplicate. Results were presented as mean values of relative enzyme inhibition (% compared to the control measurement without inhibitor) with standard deviations. During the assays, the final DMSO concentration in the wells was <2%.

IC₅₀ determination. To determine IC₅₀, the relative activity of the investigated proteases was assessed in at least 11 different concentrations of selected inhibitors. Initial compound concentrations were found experimentally. Serial dilutions of inhibitors in assay buffers (described above) were prepared in 96-well plates (20 μL of each dilution in wells). For SARS-CoV-2 PL^{Pro}, 60 μL enzyme preincubated for 10 min at 37 °C in assay buffer was added to the wells. The enzyme was incubated with inhibitors for 30 min at 37 °C. Next, 20 μL substrate (Ac-LRGG-ACC) in assay buffer was added to the wells. Final concentrations were 100 nM enzyme and 10 μM substrate. For SARS-CoV-2 M^{Pro}, 60 μL enzyme was added with no preincubation. The enzyme was incubated with inhibitor for 2 min at room temperature. Next, 20 μL of substrate (QS1) in the assay buffer was added to the wells. Final concentrations were 100 nM for the enzyme and 50 μM for the substrate. Measurements were carried out at 37 °C using a Molecular Devices Spectramax Gemini XPS spectrofluorometer. ACC fluorophore release was monitored for 30 min ($\lambda_{\text{ex}} = 355$ nm, $\lambda_{\text{em}} = 460$ nm). IC₅₀ values were determined with GraphPad Prism software using non-linear regression (dose–response—Inhibition equation) and presented as relative enzyme activity vs. inhibitor concentration. Measurements were performed at least in triplicate. Results are presented as mean values with standard deviations. During the assays, the DMSO concentration in wells was <2%. See Supplementary Information for IC₅₀ graphs.

IC₅₀ determination with nsp14 N7-MTase. To determine IC₅₀ parameters of ebselen analogs towards the nsp14 enzyme, we used the previously described Py-FLINT assay designed for N7-MTase activity studies^{42,67}. The Py-FLINT probe (1 μM) was incubated with SAM cosubstrate (20 μM), nsp14 (40 nM), and an inhibitor (half-log dilutions $\log C_{\text{inh}} < -2.5$; $2 >$). Point fluorescence measurements ($\lambda_{\text{ex}} = 345$ nm, $\lambda_{\text{em}} = 378$ nm) were carried out in 96-well black, non-binding assay plates at 30 °C. Initial rates *V* were calculated by fitting a linear curve to the first 10 points (10 min). To the obtained dependences $V(C_{\text{inh}})$ the following four-parameter dose–response equation was fitted:

$$\frac{V}{V_0} = A1 + \frac{A2 - A1}{1 + \left(\frac{C_{inh}}{IC_{50}}\right)^p}, \quad (1)$$

where A1 and A2 are the bottom and top asymptotes, respectively; C_{inh} the inhibitor concentration; p is the Hill coefficient, and V/V_0 is the ratio of the initial reaction rate with the inhibitor to that without the inhibitor. For curve fitting and IC_{50} calculations we used GraphPad Prism software.

Anti-SARS-CoV-2 and cytotoxicity assays in Vero E6 cells. The anti-SARS-CoV-2 activity was measured by determining the extent to which the compounds inhibited the virus-induced cytopathic effect (CPE) and reduced SARS-CoV-2 RNA in Vero E6 cells (ECACC 85020206). For the CPE-based assay, two-fold serial dilutions of compounds were added in triplicate in a 384-well plate with 5000 Vero E6 cells in DMEM medium with 2% FBS, 100 U of penicillin/mL, and 100 µg of streptomycin/mL (all Merck). After 1 h incubation, SARS-CoV-2 (strain hCoV-19/Czech Republic/NRL_6632_2/2020 was isolated in a biosafety level 3 laboratory from nasopharyngeal swab by inoculating Vero CCL81 cells [ECACC 84113001]) was added at multiplicity of infection 0.05 IU/mL. Following three days incubation at 37 °C in 5% CO₂, the cell viability was determined by addition of XTT solution (Sigma-Aldrich) for 4 h and the absorbance was measured using EnVision plate reader (Perkin Elmer). Drug concentrations required to reduce viral cytopathic effect by 50% (EC_{50}) were calculated using nonlinear regression from plots of percentage cell viability versus \log_{10} drug concentration using GraphPad Prism v.9.0.0 Software. For RNA reduction-based assay, two-fold serial dilutions of compounds were added in triplicate in 96-well plate with 20,000 Vero cells plated day before in the same medium as above. After 1 h incubation, SARS-CoV-2 was added at multiplicity of infection 0.05 IU/cell. After 2 h, virus was removed and new compound was added to the cells. Cells were incubated for two days, then the medium was used as a template in RT-qPCR (Multiplex RT-PCR for COVID-19, Diana Biotechnologies, Czech Republic). Compound concentrations required to reduce SARS-CoV-2 RNA copy number by 50% (EC_{50}) were calculated from plots of percentage of RNA copy number versus \log_{10} drug concentration as above.

Maximal titer reduction for selected compounds was determined at EC_{90} concentration that was computed from EC_{50} determinations using equation $EC_{90} = 9^{1/H} \times EC_{50}$, where H is Hill slope. Briefly, EC_{90} concentration of selected compounds were added in triplicate to 20,000 Vero E6 cells seeded 24 h before, incubated for 1 h and SARS-CoV-2 at MOI = 0.05 IU/mL was added. After 1 h incubation at 37 °C, 5% CO₂ medium was removed and fresh compounds at EC_{90} were added and incubated for 48 h at 37 °C, 5% CO₂. Remdesivir was included as control. Titer reduction was determined by plaque assay in Vero E6 cells. Briefly, virus supernatant was removed, tenfold serially diluted in 24-well plate followed by addition of 300,000 Vero E6 cells and 4 h incubation at 37 °C, 5% CO₂. Then, the suspension was overlaid with 1.5% (w/v) carboxymethylcellulose in DMEM and incubated for 5 days at 37 °C, 5% CO₂. After incubation, the cells were washed once with 1 × PBS, stained with naphthalene black for 45 min, washed with ddH₂O and air-dried. Plaques were counted and difference between no drug control and compound virus titer was expressed as \log_{10} plaque forming units (PFU) per mL.

Cytotoxicity was evaluated by incubating two-fold serial dilutions of each compound with Vero E6 cells. Following three days incubation at 37 °C in 5% CO₂, the cell viability was determined by addition of XTT solution as above. The compound concentrations resulting in 50% reduction of absorbance (CC_{50}) were calculated from plots of percentage of absorbance versus \log_{10} drug concentration as above.

Data availability

The datasets used and/or analysed during the current study available from the corresponding author on reasonable request.

Received: 11 April 2022; Accepted: 25 May 2023

Published online: 06 June 2023

References

- Wang, C. *et al.* A novel coronavirus outbreak of global health concern. *Lancet* **395**(10223), 470–473 (2020).
- Wu, F. *et al.* A new coronavirus associated with human respiratory disease in China. *Nature* **579**(7798), 265–269 (2020).
- Andersen, K. G. *et al.* The proximal origin of SARS-CoV-2. *Nat. Med.* **26**(4), 450–452 (2020).
- Dong, E., Du, H. & Gardner, L. An interactive web-based dashboard to track COVID-19 in real time. *Lancet Infect. Dis.* **20**(5), 533–534 (2020).
- Harvey, W. T. *et al.* SARS-CoV-2 variants, spike mutations and immune escape. *Nat. Rev. Microbiol.* **19**(7), 409–424 (2021).
- Heinz, F. X. & Stiasny, K. Distinguishing features of current COVID-19 vaccines: Knowns and unknowns of antigen presentation and modes of action. *NPJ Vaccines* **6**(1), 104 (2021).
- Zumla, A. *et al.* Coronaviruses—Drug discovery and therapeutic options. *Nat. Rev. Drug Discov.* **15**(5), 327–347 (2016).
- Elfiky, A. A. Ribavirin, remdesivir, sofosbuvir, galidesivir, and tenofovir against SARS-CoV-2 RNA dependent RNA polymerase (RdRp): A molecular docking study. *Life Sci.* **253**, 117592 (2020).
- Jin, Z. *et al.* Structure of M(pro) from SARS-CoV-2 and discovery of its inhibitors. *Nature* **582**(7811), 289–293 (2020).
- Kandeel, M. & Al-Nazawi, M. Virtual screening and repurposing of FDA approved drugs against COVID-19 main protease. *Life Sci.* **251**, 117627 (2020).
- Khodadadi, E. *et al.* Study of combining virtual screening and antiviral treatments of the Sars-CoV-2 (Covid-19). *Microb. Pathog.* **146**, 104241 (2020).
- Rameshrad, M. *et al.* A comprehensive review on drug repositioning against coronavirus disease 2019 (COVID19). *Naunyn Schmiedeberg's Arch. Pharmacol.* **393**(7), 1137–1152 (2020).
- Joshi, S., Joshi, M. & Degani, M. S. Tackling SARS-CoV-2: Proposed targets and repurposed drugs. *Future Med. Chem.* **12**(17), 1579–1601 (2020).
- Beigel, J. H. *et al.* Remdesivir for the treatment of Covid-19—Final report. *N. Engl. J. Med.* **383**(19), 1813–1826 (2020).

15. WHO ST Consortium. Repurposed antiviral drugs for Covid-19—Interim WHO solidarity trial results. *N. Engl. J. Med.* **384**(6), 497–511 (2021).
16. Fehr, A. R. & Perlman, S. Coronaviruses: An overview of their replication and pathogenesis. *Methods Mol. Biol.* **1282**, 1–23 (2015).
17. Hilgenfeld, R. From SARS to MERS: Crystallographic studies on coronaviral proteases enable antiviral drug design. *FEBS J.* **281**(18), 4085–4096 (2014).
18. Zhang, L. *et al.* Crystal structure of SARS-CoV-2 main protease provides a basis for design of improved alpha-ketoamide inhibitors. *Science* **368**(6489), 409–412 (2020).
19. Anand, K. *et al.* Coronavirus main proteinase (3CLpro) structure: Basis for design of anti-SARS drugs. *Science* **300**(5626), 1763–1767 (2003).
20. Fan, K. *et al.* Biosynthesis, purification, and substrate specificity of severe acute respiratory syndrome coronavirus 3C-like proteinase. *J. Biol. Chem.* **279**(3), 1637–1642 (2004).
21. Goyal, B. & Goyal, D. Targeting the dimerization of the main protease of coronaviruses: A potential broad-spectrum therapeutic strategy. *ACS Combin. Sci.* **22**(6), 297–305 (2020).
22. Rut, W. *et al.* SARS-CoV-2 M(pro) inhibitors and activity-based probes for patient-sample imaging. *Nat. Chem. Biol.* **17**(2), 222–228 (2021).
23. Yang, H. *et al.* Design of wide-spectrum inhibitors targeting coronavirus main proteases. *PLoS Biol.* **3**(10), e324 (2005).
24. Freitas, B. T. *et al.* Characterization and noncovalent inhibition of the deubiquitinase and deISGylase activity of SARS-CoV-2 papain-like protease. *ACS Infect. Dis.* **6**(8), 2099–2109 (2020).
25. Klemm, T. *et al.* Mechanism and inhibition of the papain-like protease, PLpro, of SARS-CoV-2. *EMBO J.* **39**(18), e106275 (2020).
26. Rut, W. *et al.* Activity profiling and crystal structures of inhibitor-bound SARS-CoV-2 papain-like protease: A framework for anti-COVID-19 drug design. *Sci. Adv.* **6**(42), eabd4596 (2020).
27. Shin, D. *et al.* Papain-like protease regulates SARS-CoV-2 viral spread and innate immunity. *Nature* **587**(7835), 657–662 (2020).
28. Lesser, R. & Weiß, R. Über selenhaltige aromatische Verbindungen (VI). *Ber. dtsh. Chem. Ges. A/B* **57**, 1077–1082 (1924).
29. Muges, G., du Mont, W. W. & Sies, H. Chemistry of biologically important synthetic organoselenium compounds. *Chem. Rev.* **101**(7), 2125–2179 (2001).
30. Antony, S. & Bayse, C. A. Modeling the mechanism of the glutathione peroxidase mimic ebselen. *Inorg. Chem.* **50**(23), 12075–12084 (2011).
31. Azad, G. K. & Tomar, R. S. Ebselen, a promising antioxidant drug: Mechanisms of action and targets of biological pathways. *Mol. Biol. Rep.* **41**(8), 4865–4879 (2014).
32. Sarma, B. K. & Muges, G. Antioxidant activity of the anti-inflammatory compound ebselen: A reversible cyclization pathway via selenenic and seleninic acid intermediates. *Chemistry* **14**(34), 10603–10614 (2008).
33. Bhabak, K. P. & Muges, G. Functional mimics of glutathione peroxidase: Bioinspired synthetic antioxidants. *Acc. Chem. Res.* **43**(11), 1408–1419 (2010).
34. Morgenstern, R., Cotgreave, I. A. & Engman, L. Determination of the relative contributions of the diselenide and selenol forms of ebselen in the mechanism of its glutathione peroxidase-like activity. *Chem. Biol. Interact.* **84**(1), 77–84 (1992).
35. Sands, K. N. & Back, T. G. Key steps and intermediates in the catalytic mechanism for the reduction of peroxides by the antioxidant ebselen. *Tetrahedron* **74**(38), 4959–4967 (2018).
36. Sies, H. Ebselen, a selenoorganic compound as glutathione peroxidase mimic. *Free Radic. Biol. Med.* **14**(3), 313–323 (1993).
37. Wedding, J. L. *et al.* Investigation into the intracellular fates, speciation and mode of action of selenium-containing neuroprotective agents using XAS and XFM. *Biochim. Biophys. Acta Gen. Subj.* **1862**(11), 2393–2404 (2018).
38. Weglarz-Tomczak, E. *et al.* Identification of ebselen and its analogues as potent covalent inhibitors of papain-like protease from SARS-CoV-2. *Sci. Rep.* **11**(1), 3640 (2021).
39. Ampornnanai, K. *et al.* Inhibition mechanism of SARS-CoV-2 main protease by ebselen and its derivatives. *Nat. Commun.* **12**(1), 3061 (2021).
40. Cao, J., Forrest, J. C. & Zhang, X. A screen of the NIH Clinical Collection small molecule library identifies potential anti-coronavirus drugs. *Antivir. Res.* **114**, 1–10 (2015).
41. Mangiacavchi, F. *et al.* Seleno-functionalization of quercetin improves the non-covalent inhibition of M(pro) and its antiviral activity in cells against SARS-CoV-2. *Int. J. Mol. Sci.* **22**(13), 7048 (2021).
42. Kasprzyk, R. *et al.* Identification and evaluation of potential SARS-CoV-2 antiviral agents targeting mRNA cap guanine N7-Methyltransferase. *Antivir. Res.* **193**, 105142 (2021).
43. Chen, Y. *et al.* Functional screen reveals SARS coronavirus nonstructural protein nsp14 as a novel cap N7 methyltransferase. *Proc. Natl. Acad. Sci. U.S.A.* **106**(9), 3484–3489 (2009).
44. Bouvet, M. *et al.* In vitro reconstitution of SARS-coronavirus mRNA cap methylation. *PLoS Pathog.* **6**(4), e1000863 (2010).
45. Dong, H., Zhang, B. & Shi, P. Y. Flavivirus methyltransferase: A novel antiviral target. *Antivir. Res.* **80**(1), 1–10 (2008).
46. Tong, T. R. Drug targets in severe acute respiratory syndrome (SARS) virus and other coronavirus infections. *Infect. Disord. Drug Targets* **9**(2), 223–245 (2009).
47. Hartenian, E. *et al.* The molecular virology of coronaviruses. *J. Biol. Chem.* **295**(37), 12910–12934 (2020).
48. Malone, B. *et al.* Structures and functions of coronavirus replication-transcription complexes and their relevance for SARS-CoV-2 drug design. *Nat. Rev. Mol. Cell Biol.* **23**(1), 21–39 (2022).
49. Sancineto, L. *et al.* Design and synthesis of DiselenoBisBenzamides (DISEBAs) as nucleocapsid protein 7 (NCp7) inhibitors with anti-HIV activity. *J. Med. Chem.* **58**(24), 9601–9614 (2015).
50. Thenin-Houssier, S. *et al.* Ebselen, a small-molecule capsid inhibitor of HIV-1 replication. *Antimicrob. Agents Chemother.* **60**(4), 2195–2208 (2016).
51. Sartori, G. *et al.* Antiviral action of diphenyl diselenide on herpes simplex virus 2 infection in female BALB/c mice. *J. Cell. Biochem.* **117**(7), 1638–1648 (2016).
52. Mukherjee, S. *et al.* Ebselen inhibits hepatitis C virus NS3 helicase binding to nucleic acid and prevents viral replication. *ACS Chem. Biol.* **9**(10), 2393–2403 (2014).
53. Simanjuntak, Y. *et al.* Ebselen alleviates testicular pathology in mice with Zika virus infection and prevents its sexual transmission. *PLoS Pathog.* **14**(2), e1006854 (2018).
54. Zhao, R. & Holmgren, A. A novel antioxidant mechanism of ebselen involving ebselen diselenide, a substrate of mammalian thioredoxin and thioredoxin reductase. *J. Biol. Chem.* **277**(42), 39456–39462 (2002).
55. Azeredo, J. B., Schwab, R. S. & Braga, A. L. Synthesis of biologically active selenium-containing molecules from greener perspectives. *Curr. Green Chem.* **3**(1), 51–67 (2016).
56. Balkrishna, S. J. *et al.* An ebselen like catalyst with enhanced GPx activity via a selenol intermediate. *Org. Biomol. Chem.* **12**(8), 1215–1219 (2014).
57. Balkrishna, S. J. *et al.* Cu-catalyzed efficient synthetic methodology for ebselen and related Se-N heterocycles. *Org. Lett.* **12**(23), 5394–5397 (2010).
58. Balkrishna, S. J., Bhakuni, B. S. & Kumar, S. Copper catalyzed/mediated synthetic methodology for ebselen and related isoselenazolones. *Tetrahedron* **67**(49), 9565–9575 (2011).
59. Osajda, M. & Młochowski, J. The reactions of 2-(chloroseleno)benzoyl chloride with nucleophiles. *Tetrahedron* **58**(37), 7531–7537 (2002).

60. Giurg, M. *et al.* Reaction of bis[(2-chlorocarbonyl)phenyl] diselenide with phenols, aminophenols, and other amines towards diphenyl diselenides with antimicrobial and antiviral properties. *Molecules* **22**(6), 974 (2017).
61. Mlochowski, J. *et al.* Synthesis and properties of 2-carboxyalkyl-1,2-benzisoselenazol-3(2H)-ones and related organoselenium compounds as nitric oxide synthase inhibitors and cytokine inducers. *Liebigs Ann.* **1996**(11), 1751–1755 (1996).
62. Giurg, M. & Syper, L. Diaryl diselenides and related compounds as oxygen-transfer agents. *Phosphorus Sulfur Silicon Relat. Elem.* **183**(4), 970–985 (2008).
63. Piętko-Ottlik, M. *et al.* Synthesis of new alkylated and methoxylated analogues of ebselen with antiviral and antimicrobial properties. *ARKIVOC* **2017**(2), 546–556 (2017).
64. Weglarz-Tomczak, E. *et al.* Identification of methionine aminopeptidase 2 as a molecular target of the organoselenium drug ebselen and its derivatives/analogues: Synthesis, inhibitory activity and molecular modeling study. *Bioorg. Med. Chem. Lett.* **26**(21), 5254–5259 (2016).
65. Bernatowicz, P. *et al.* A ¹³C, ¹⁵N and ⁷⁷Se NMR study of some seleno and diseleno azines and related compounds. *Pol. J. Chem.* **71**, 441–445 (1997).
66. Pacula, A. J., Ścianowski, J. & Aleksandrak, K. B. Highly efficient synthesis and antioxidant capacity of N-substituted benzisoselenazol-3(2H)-ones. *RSC Adv.* **4**(90), 48959–48962 (2014).
67. Kasprzyk, R. *et al.* Direct high-throughput screening assay for mRNA cap guanine-N7 methyltransferase activity. *Chemistry* **26**(49), 11266–11275 (2020).
68. Delgado-Roche, L. & Mesta, F. Oxidative stress as key player in severe acute respiratory syndrome coronavirus (SARS-CoV) infection. *Arch. Med. Res.* **51**(5), 384–387 (2020).
69. Takayama, K. In vitro and animal models for SARS-CoV-2 research. *Trends Pharmacol. Sci.* **41**(8), 513–517 (2020).
70. Menendez, C. A. *et al.* Molecular characterization of ebselen binding activity to SARS-CoV-2 main protease. *Sci. Adv.* **6**(37), eabd0345 (2020).
71. Qiao, Z. *et al.* The Mpro structure-based modifications of ebselen derivatives for improved antiviral activity against SARS-CoV-2 virus. *Bioorg. Chem.* **117**, 105455 (2021).
72. Ma, C. *et al.* Ebselen, disulfiram, carmofur, PX-12, tideglusib, and shikonin are nonspecific promiscuous SARS-CoV-2 main protease inhibitors. *ACS Pharmacol. Transl. Sci.* **3**(6), 1265–1277 (2020).
73. Ma, C. *et al.* Validation and invalidation of SARS-CoV-2 main protease inhibitors using the Flip-GFP and Protease-Glo luciferase assays. *Acta Pharm. Sin. B* **12**(4), 1636–1651 (2022).
74. Tan, H., Ma, C. & Wang, J. Invalidation of dieckol and 1,2,3,4,6-pentagalloylglucose (PGG) as SARS-CoV-2 main protease inhibitors and the discovery of PGG as a papain-like protease inhibitor. *Med. Chem. Res.* **31**(7), 1147–1153 (2022).
75. Heilmann, E. *et al.* A VSV-based assay quantifies coronavirus Mpro/3CLpro/Nsp5 main protease activity and chemical inhibition. *Commun. Biol.* **5**(1), 391 (2022).
76. Nogueira, C. W., Barbosa, N. V. & Rocha, J. B. T. Toxicology and pharmacology of synthetic organoselenium compounds: An update. *Arch. Toxicol.* **95**(4), 1179–1226 (2021).
77. Suhail, S. *et al.* Role of oxidative stress on SARS-CoV (SARS) and SARS-CoV-2 (COVID-19) infection: A review. *Protein J.* **39**(6), 644–656 (2020).
78. Taylor, E. W. & Radding, W. Understanding selenium and glutathione as antiviral factors in COVID-19: Does the viral M(pro) protease target host selenoproteins and glutathione synthesis?. *Front. Nutr.* **7**, 143 (2020).
79. Du, L. *et al.* Oxidative stress transforms 3CLpro into an insoluble and more active form to promote SARS-CoV-2 replication. *Redox. Biol.* **48**, 102199 (2021).
80. Lynch, E. & Kil, J. Development of ebselen, a glutathione peroxidase mimic, for the prevention and treatment of noise-induced hearing loss. *Semin. Hear.* **30**(01), 047–055 (2009).
81. Sharpley, A. L. *et al.* A phase 2a randomised, double-blind, placebo-controlled, parallel-group, add-on clinical trial of ebselen (SPI-1005) as a novel treatment for mania or hypomania. *Psychopharmacology* **237**(12), 3773–3782 (2020).
82. Yamaguchi, T. *et al.* Ebselen in acute ischemic stroke: A placebo-controlled, double-blind clinical trial. Ebselen Study Group. *Stroke* **29**(1), 12–17 (1998).
83. Singh, N. *et al.* A safe lithium mimetic for bipolar disorder. *Nat. Commun.* **4**, 1332 (2013).
84. Granda, J. *et al.* Synthesis of 7- and 8-functionalized 2-aminophenoxazinones via cyclocondensation of 2-aminophenols. *Synthesis* **47**(21), 3321–3332 (2015).
85. Welter, A., Christiaens, L. & Wirtz-Peitz, F. Benzisoselenazolones and processes for the treatment of rheumatic and arthritic diseases using them (1983).
86. Mlochowski, J. *et al.* Aromatic and azaaromatic diselenides, benzisoselenazolones and related compounds as immunomodulators active in humans: Synthesis and properties. *Liebigs Ann. Chem.* **1993**(12), 1239–1244 (1993).
87. Welter, A. *et al.* Diselenobis-benzoic acid amides of primary and secondary amines and processes for the treatment of diseases in humans caused by a cell injury (1989).
88. Kuppers, J. *et al.* Convergent synthesis of two fluorescent ebselen-coumarin heterodimers. *Pharmaceuticals (Basel)* **9**(3), 43 (2016).
89. Chang, T. C. *et al.* Synthesis and biological evaluation of ebselen and its acyclic derivatives. *Chem. Pharm. Bull. (Tokyo)* **51**(12), 1413–1416 (2003).
90. Gustafsson, T. N. *et al.* Ebselen and analogs as inhibitors of *Bacillus anthracis* thioredoxin reductase and bactericidal antibacterials targeting *Bacillus* species, *Staphylococcus aureus* and *Mycobacterium tuberculosis*. *Biochim. Biophys. Acta* **1860**(6), 1265–1271 (2016).
91. Wan, J. *et al.* Benzisoselenazole ketone compound and application thereof and bactericide (2021).
92. Bender, C. O. *et al.* Use of small molecules for the treatment of *Clostridium difficile* toxicity (2015).
93. Garland, M. *et al.* Covalent modifiers of botulinum neurotoxin counteract toxin persistence. *ACS Chem. Biol.* **14**(1), 76–87 (2019).
94. Xue, X. *et al.* Production of authentic SARS-CoV M(pro) with enhanced activity: Application as a novel tag-cleavage endopeptidase for protein overproduction. *J. Mol. Biol.* **366**(3), 965–975 (2007).

Acknowledgements

This work was supported by the Medical Research Agency in Poland through its Own Project (grant 2020/ABM/SARS/1) and by the National Science Centre in Poland grant number (2020/01/0/NZ1/00063) to M.D. and (UMO-2020/01/0/ST4/00124) to J.J. The Drag laboratory is supported by the "TEAM/2017-4/32" project, which is conducted within the TEAM programme of the Foundation for Polish Science cofinanced by the European Union under the European Regional Development Fund. Work in the Hilgenfeld laboratory was supported by the SCORE project of the European Union (grant agreement # 101003627), by the German Center for Infection Research (DZIF), and by the Government of Schleswig-Holstein through its Structure and Excellence Fund, as well as by a close partnership between the Possehl Foundation (Lübeck) and the University of Lübeck. The anti-SARS-CoV-2 activity determination was supported by ERDF/ESF project ChemBioDrug CZ.02.1.01/0.0/0.0/16_019/0000729 and the Institute of Organic Chemistry and Biochemistry of the CAS (RVO 61388963). The

Olsen laboratory is supported by CPRIT RR200030 and NIH R01 GM115568 and GM128731. We are thankful to Wroclaw University of Science and Technology for support for the Department of Organic and Medicinal Chemistry—K20 (Statute Funds 82013902).

Author contributions

M.Z. and M.D. designed the research; M.Z., W.R. and M.Zg. performed the research and collected data; K.O., J.G., M.G. and M.B.-G. synthesized and provided the collection of compounds, M.K.-B., L.Z., X.S. and R.H. provided SARS-CoV-2 M^{Pro} enzyme; Z.L., D.N. and S.K.O. provided SARS-CoV-2 PL^{Pro} enzyme, M.Z., W.R. and J.W. analyzed and interpreted the inhibitory data and M.Z. wrote the manuscript; all authors critically revised the manuscript.

Competing interests

The authors declare no competing interests.

Additional information

Supplementary Information The online version contains supplementary material available at <https://doi.org/10.1038/s41598-023-35907-w>.

Correspondence and requests for materials should be addressed to M.Z. or M.D.

Reprints and permissions information is available at www.nature.com/reprints.

Publisher's note Springer Nature remains neutral with regard to jurisdictional claims in published maps and institutional affiliations.



Open Access This article is licensed under a Creative Commons Attribution 4.0 International License, which permits use, sharing, adaptation, distribution and reproduction in any medium or format, as long as you give appropriate credit to the original author(s) and the source, provide a link to the Creative Commons licence, and indicate if changes were made. The images or other third party material in this article are included in the article's Creative Commons licence, unless indicated otherwise in a credit line to the material. If material is not included in the article's Creative Commons licence and your intended use is not permitted by statutory regulation or exceeds the permitted use, you will need to obtain permission directly from the copyright holder. To view a copy of this licence, visit <http://creativecommons.org/licenses/by/4.0/>.

© The Author(s) 2023